

Trajectory Characters of Rogue Waves

Liming Ling¹, Li-Chen Zhao^{1,2*}

¹*Institute of Applied Physics and Computational Mathematics, Beijing 100088, China and*

²*Department of Modern Physics, University of Science and Technology of China, Hefei 230026, China*

(Dated: September 29, 2019)

We present a simple representation for arbitrary-order rogue wave solution and study on the trajectories of them explicitly. We find that the global trajectories on temporal-spatial distribution all look like “X” shape for rogue waves. Short-time prediction on rogue wave can be done through measuring the information contained in the initial perturbation twice.

PACS numbers: 03.75.Kk, 03.75.lm, 67.85.Hj

I. INTRODUCTION

Rogue waves (RW) are both localized in space and time and depict a unique event which seems to appear from nowhere and disappear without a trace [1–5]. They are one of those fascinating destructive phenomena in nature, and have been observed experimentally in nonlinear optics [6] and water wave tank [7]. Many studies indicate that nonlinear theories can be used to explain the dramatic phenomena. Among nonlinear theories, the most fundamental is based on the nonlinear Schrödinger equation (NLS) [8]

$$i \frac{\partial u(x, t)}{\partial t} + \frac{\partial^2 u(x, t)}{\partial x^2} + 2|u(x, t)|^2 u(x, t) = 0, \quad (1)$$

whose rational solution has been used to describe the RW phenomena [9].

Most studies focus on the highest peak value and the structure character when the highest peak emerge [10–12], since RW seems to appear from nowhere and disappear without a trace. In fact, RW always contain certain structure on the plain background, and its trajectory indeed exist. The perturbation is so weak that it can not be observed clearly long before or after the moment when the highest peak emerges. We can study its trajectory based on the RW solution. The knowledge about its traces would help us to predict and prevent RW phenomena.

In this paper, we present a simple representation for general NLS RW solution, and investigate the dynamics and kinetics of RW explicitly. We find the whole trajectories for high-order RWs are similar to the one of the first-order RW, whose trajectory looks like an “X”. They are different around the location where the RW happens. For first-order RW, we can predict the location on temporal-spatial distribution where it will appear by testing the width and hump of RW twice. The results can be extended to predict the higher-order RW.

II. A SIMPLE REPRESENTATION FOR GENERAL ROGUE WAVE SOLUTION

We derive a generalized expression for arbitrary Nth-order RW solution of Eq. (1) as follows

Theorem 1

$$u(x, t) = \left(1 - 2 \frac{\det(A_1)}{\det(A)} \right) \exp(2it), \quad (2)$$

and its density expression can be derived as

$$|u|^2 = 1 + 2i \left(\frac{\det(A_2)}{\det(A)} \right)_x. \quad (3)$$

The expressions for A_1 , A_2 and A are

$$\begin{aligned} A_1 &= \begin{pmatrix} A & A_1[2] \\ A_1[1] & 0 \end{pmatrix}, \\ A_2 &= \begin{pmatrix} A & A_2[2] \\ A_2[1] & 0 \end{pmatrix}, \\ A &= (A_{i,j})_{1 \leq i, j \leq N}, \end{aligned} \quad (4)$$

where

$$\begin{aligned} A_1[1] &= [\phi_0, \phi_1, \dots, \phi_{N-1}], & A_1[2] &= [\bar{\psi}_0, \bar{\psi}_1, \dots, \bar{\psi}_{N-1}]^T, \\ A_2[1] &= [\psi_0, \psi_1, \dots, \psi_{N-1}], & A_2[2] &= A_1[2]. \end{aligned}$$

The variable function ψ_j , ϕ_j and $A_{i,j}$ are the related Taylor expansion coefficients of the following functions

$$\begin{aligned} \psi &= i(C_1 X - C_2 X^{-1}) \equiv \sum_{i=0}^{+\infty} \psi_i f^{2i}, \\ \phi &= C_2 X - C_1 X^{-1} \equiv \sum_{i=0}^{+\infty} \phi_i f^{2i}, \\ A(f, g) &= \frac{i(\psi \bar{\psi} + \phi \bar{\phi})}{2 + f^2 + \bar{f}^2} = \sum_{i,j=0}^{+\infty, +\infty} A_{i,j} f^{2i} \bar{f}^{2j}, \end{aligned} \quad (5)$$

where $C_1 = \frac{\sqrt{1+f^2-h}}{h}$, $C_2 = \frac{\sqrt{1+f^2+h}}{h}$, $X = e^{h[x+2it+2itf^2+s(f)]}$, $h = f\sqrt{2+f^2}$, and $s(f) = \sum_{i=1}^{N-1} s_i f^{2i}$ (s_i is a complex constant). The symbol $\bar{}$ represents the complex conjugation.

*Electronic address: zhaolichen3@163.com

Proof: We prove this theorem based on generalized Darboux transformation. We neglect the proof for the generalized Darboux transformation, since the details are given in references [13–17]. The Lax pair for NLS equation (1) is:

$$\begin{aligned}\Psi_x &= (-i\lambda\sigma_3 + iQ)\Psi, \\ \Psi_t &= (2i\lambda^2\sigma_3 - 2i\lambda Q - i\sigma_3 Q^2 + \sigma_3 Q_x)\Psi,\end{aligned}\quad (6)$$

where

$$\sigma_3 = \begin{pmatrix} 1 & 0 \\ 0 & -1 \end{pmatrix}, \quad Q = \begin{pmatrix} 0 & u^* \\ u & 0 \end{pmatrix}.$$

Suppose the seed solution for NLS equation (1) is $u[0] = \exp[2it]$, then we have the fundamental solution for Lax pair (6)

$$\begin{aligned}\Psi_0 &= \exp[-it\sigma_3] \begin{pmatrix} 1 & 0 \\ \lambda - \sqrt{1+\lambda^2} & 1 \end{pmatrix} \begin{pmatrix} \sqrt{1+\lambda^2} - \lambda \\ 1 \end{pmatrix} \\ &\cdot \exp[-i(1+\lambda^2)^{1/2}(x-2\lambda t)\sigma].\end{aligned}\quad (7)$$

Together with the generalized Darboux transformation T , we can obtain the fundamental solution matrix $\Psi = T\Psi_0$ for general rogue wave solution u . On the other hand, we can see that

$$\Psi = E \exp[-i\lambda\sigma_3(x-2\lambda t)], \quad \text{as } \lambda \rightarrow \infty^+,$$

here $E = I + E_1\lambda^{-1} + E_2\lambda^{-2} + O(\lambda^{-3})$. Then we have

$$\begin{aligned}E_x &= -i\lambda[\sigma_3, E] + iQE, \\ E_t &= 2i\lambda^2[\sigma_3, E] + (-2i\lambda Q - i\sigma_3 Q^2 + \sigma_3 Q_x)E.\end{aligned}$$

Comparing the coefficient of above two equations, then we have

$$\begin{aligned}Q &= [\sigma_3, E_1], \\ E_{1,x} &= -i[\sigma_3, E_2] + iQE_1, \\ 2i[\sigma_3, E_2] - i\sigma_3 Q^2 + \sigma_3 Q_x - 2iQE_1 &= 0.\end{aligned}$$

It follows that we have

$$\sigma_3 Q^2 = 2iE_{1,x}^{diag}.$$

The Taylor expansion

$$\sqrt{1+\lambda^2} = \lambda + \frac{1}{2}\lambda^{-1} - \frac{1}{8}\lambda^{-3} + O(\lambda^{-5})$$

and

$$T = I + \sum_{i=1}^N \frac{T_i}{\lambda - \lambda_i}$$

give the exact formula for u and $|u|^2$:

$$\begin{aligned}u &= \exp(2it) - 2 \sum_{i=1}^N T_i[21], \\ |u|^2 &= 1 + 2i \left(\sum_{i=1}^N T_i[11] \right)_x,\end{aligned}$$

where $T_i[11]$ and $T_i[21]$ represent the (1, 1) and (2, 1) element of matrix T_i respectively. Finally, the exact rogue wave solution can be obtained by the limit technique [13, 14]. \square

We illustrate that we give a simple formula of general rogue wave solution for NLS equation (1). In reference [10], the authors merely give the first five order rogue wave by modified Darboux transformation. Many different methods have been performed to derive Nth-order RW solution, such as the Hirota bilinear method [11], reduction method [18], algebraic reduction method [19, 20], and the generalized Darboux transformation method [12]. However, the formulas presented in these papers are all the ratio of two $2N \times 2N$ determinants. In this paper, we develop the generalized Darboux transformation method [12] to present a much simpler representation for Nth-order RWs with ratio of $(N+1) \times (N+1)$ order determinant and $N \times N$ order determinant.

III. THE DYNAMICS AND KINETICS OF FUNDAMENTAL ROGUE WAVES

The fundamental RW solution has been given for a long time [21], and its explicit formation can be given directly from the generalized expression with $N = 1$ as

$$u[1] = \left(-1 + \frac{4(1+4it)}{1+4x^2+16t^2} \right) e^{2it}$$

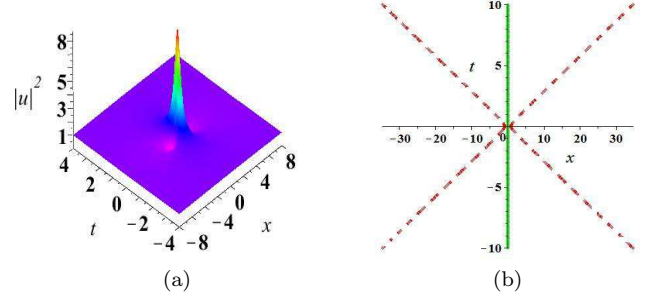


FIG. 1: (color online) (a) The trace of the first-order RW. (b) The density evolution of the first-order RW. The green solid line correspond to the trajectory of the RW’s hump and the red dashed lines correspond to the trajectories of the RW’s valleys. This holds for all pictures in the paper.

The solution corresponds to the well-known “eyes” shaped RW. Near $t = 0$, the wave has highest hump and there are two valleys around the hump (see Fig. 1(a)). Long before or after $t = 0$, the peak values of the hump and valley are close to the background. But the wave keep the structure shape before or after the moment $t = 0$. Therefore, we can define the trajectory by the motion of its hump and the valleys, which can be

described by the motion of the hump and valleys' center locations [22]. The motion of its hump's center is calculated as

$$X_h = 0, \quad (8)$$

and the motions of the two valleys' center are

$$X_v = \pm\sqrt{3}\left(t^2 + \frac{3}{48}\right)^{1/2}. \quad (9)$$

Then, we can plot the RW's trajectory in Fig. 1 (b). The trajectory looks like an "X" shape, for which there is a straight green solid line and two red dashed lines. The green solid line is the trajectory of RW's hump, and the red dashed lines are the trajectories of the two valleys. Furthermore, we can define the width of RW as the distance between the two valleys' centers, which corresponds to the distance between the two red lines in Fig. 1(b). Its evolution is

$$W = 2\sqrt{3}\left(t^2 + \frac{3}{48}\right)^{1/2}. \quad (10)$$

Obviously, the width is compressed before the moment $t = 0$ when the highest peak emerge and is broadened after the moment.

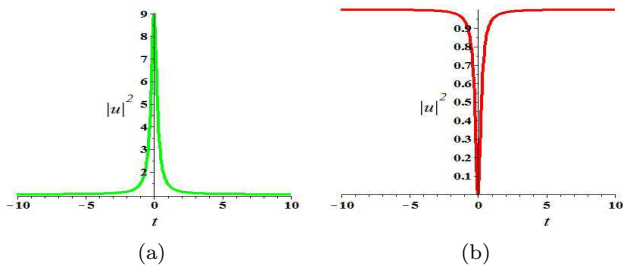


FIG. 2: (color online) (a) The value evolution of RW's peak. (b) The value evolution of RW's hole.

Correspondingly, one can derive explicit expressions directly which describe the evolution of RW's hump and valleys, shown in Fig. 2. It is seen that the highest value of the RW is nine times the value of background. Compare Fig. 1(b) and Fig. 2, we know that RW has the highest and steepest structure when the width is the smallest. Namely, modulation instability induces the compressive effect on the two valleys. The width is broaden or compressed with time, the peak decrease or increase correspondingly.

IV. SHORT-TIME PREDICTION ON ROGUE WAVES

From the evolution of RW's hump and valleys, we can know that the perturbation for RW is too weak to be tested at moments which are long before the RW emerges.

Therefore, it is very hard to predict RW long time before it emerges. However, short-time before or after the RW emerge, the perturbation is a stronger, and can be tested easier. Based on this properties, short-time prediction about them could be realized through measuring the perturbation distribution.

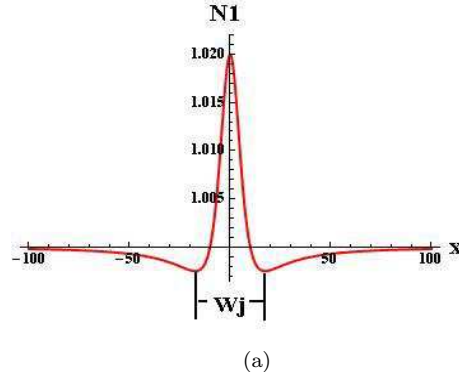


FIG. 3: (color online) The density measurement for the perturbation for RW. The width between the two valleys' centers is marked by W_j

For example, we measure the density distribution of the perturbation at a time, such as the ones in Fig. 3. One can measure the distance between the two valleys' centers, marked as W_1 . Because the symmetry of RW evolution, we need measure it again just after and next to the first measure time. The second width measurement value is marked as W_2 . If $W_2 > W_1$, the RW has emerged before we measure; if $W_2 < W_1$, the RW has not emerged and the time how long after the second measure time the highest peak will appear is $\frac{\sqrt{-3+4W_2^2}}{4\sqrt{3}}$. The location where RW emerge can be predicted by the trajectory of its hump. Since the trajectory of the hump is a straight line, we can predict the location by measuring the hump twice. Considering that two points determine one straight line and the time has been predicted, we can predict the explicit location on the temporal-spatial distribution where the highest peak emerges. Since the traces for higher-order RWs are similar, we can extend the prediction to them. It should be emphasized that the study on spectral character of optical RW has been done in [23], which indicates that the specific triangular spectra could be used to early warning for RW. We believe that there should be some corresponding relations between the spectra and trace.

V. THE TRAJECTORY FOR SECOND-ORDER ROGUE WAVE

Higher-order RW solution has been presented in [10–12]. It is known that the second order rogue wave possesses different dynamics. Choosing the parameter $s_1 = a + ib$, we can readily obtain the general second

order rogue wave solution by the formula (2)

$$u[2] = \left(1 + \frac{D_1}{D_2}\right) e^{2it},$$

$$\begin{aligned} D_1 &= (-576x - 2304ixt)a + (144i - 2304it^2 - 1152t \\ &\quad + 576ix^2)b - 768ix^4t - 192x^4 - 1536it^3 - 288x^2 \\ &\quad - 3456t^2 + 36 - 4608x^2t^2 - 12288it^5 + 720it \\ &\quad - 6144it^3x^2 + 1152ix^2t - 15360t^4, \\ D_2 &= 144a^2 + (144x - 192x^3 + 2304xt^2)a + 144b^2 \\ &\quad + (-1152x^2t + 864t + 1536t^3)b + 9 + 108x^2 + 1584t^2 \\ &\quad + 48x^4 + 6912t^4 + 768x^4t^2 + 64x^6 - 1152x^2t^2 \\ &\quad + 4096t^6 + 3072x^2t^4. \end{aligned}$$

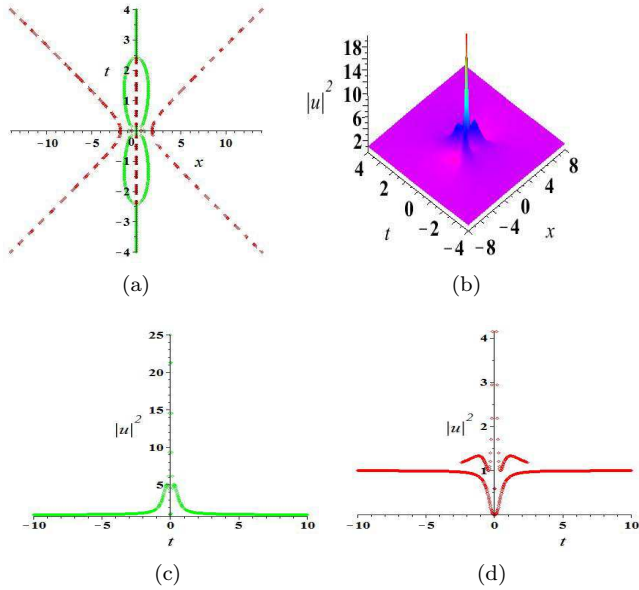


FIG. 4: (color online) (a) The trajectory of the second-order RW. (b) The density evolution of the second-order RW. (c) The value evolution of RW's hump peak. (d) The value evolution of RW's valleys.

The trajectory of first order rogue wave can be derived exactly. However, for the 2-nd rogue wave, we can not obtain exact expression for the trajectory of 2-nd rogue wave, since the high order algebraic equation emerge for these extreme points. When x or $t \rightarrow \infty$, we can readily prove that the trajectory of 2-nd order rogue wave is asymptotic to the first order rogue wave. But we can not obtain the trajectory of 2-nd rogue wave in the neighbourhood of $(x, t) = (0, 0)$ with a simple way. To give the trajectory of 2-nd rogue wave, we use the numerical method. We know that the locations of humps and valleys can be used to describe RW's trajectory. Thus we

merely need to obtain the trajectories of these extreme points.

In mathematical view, hump's center corresponds to maximum point of the density distribution function, and valley's center is the minimum point. To obtain the trajectories of them, we just need obtain the zero points of $(|u[2]|^2)_x$ and the sign of corresponding value of $(|u[2]|^2)_{xx}$ for fixed t . The first step, we solve the nonlinear equation— $(|u[2]|^2)_x = 0$ numerically to find out the extreme points. Secondly, we can classify the extreme points by the sign of $(|u[2]|^2)_{xx}$. If the sign of $(|u[2](x_0)|^2)_{xx}$ is positive, then the point x_0 is minimum point; if the sign of $(|u[2](x_0)|^2)_{xx}$ is negative, then the point x_0 is maximum point. We can plot the trajectories of higher-order RW by this way.

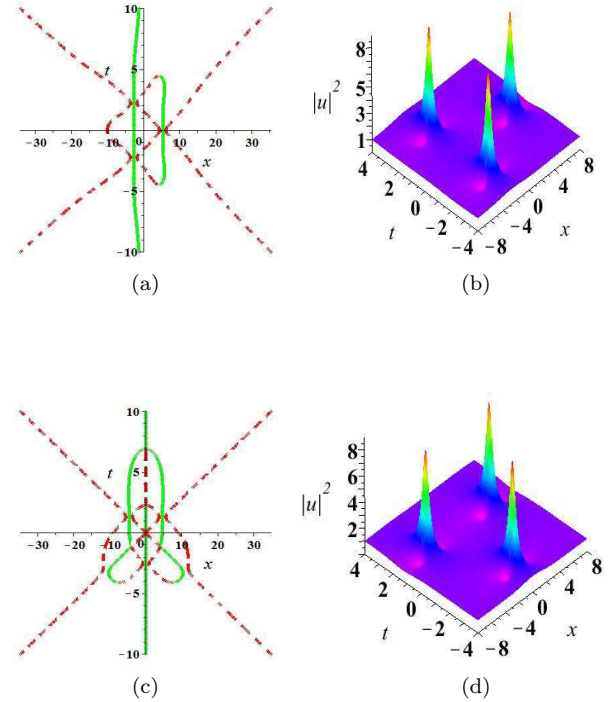


FIG. 5: (color online) (a) The trajectory of the second-order RW which is symmetrical about the x axis. (b) The density evolution of the second-order RW which is symmetrical about the x axis. (c) The trajectory of the second-order RW which is symmetrical about the t axis. (d) The density evolution of the second-order RW which is symmetrical about the t axis

We merely consider the three special cases for 2-nd rogue wave solution. Firstly, we give the trace for the standard 2-nd rogue wave solution in Fig. 4 (a) and (b), which is symmetrical about both the x and t axis. We use the numerical method to derive the peak value curve and hole value curve for standard 2-nd rogue wave (Fig. 4 (c) and (d)). Compare the trajectory in Fig. 4 with the one in Fig. 1, we know that the the whole trajectories of them are similar, but the trajectory and structures

are distinctive from each other near the location where highest peak emerges. Compare the curves in Fig. 4 (c) and (d) with Fig. 2, we can see that the two curves are very similar. But they possess different peak values. The maximum of peak value curve for 2-nd rogue wave is 25. But the maximum of peak value curve for first order rogue wave is 9. The hole value of 2-nd rogue wave is also similar with first order rogue wave. But there is a hole curve in the center lonely, which is higher than the background. The maximum of the curve is about 4.2.

For second-order RW, there can be three fundamental RWs in the temporal-spatial distribution. As examples, we give other two special cases for the trajectory of 2-nd rogue wave solution in Fig. 5, which are symmetrical about the x and t axis separately. From the pictures, we can see that the trajectory of rogue wave is consistent with the first order rogue wave. Each center of the “X” shape corresponds to the highest peak’s location. This can be verified by comparing the locations in Fig. 5. The short-time prediction discussions on the first-order RW are applicable on them too.

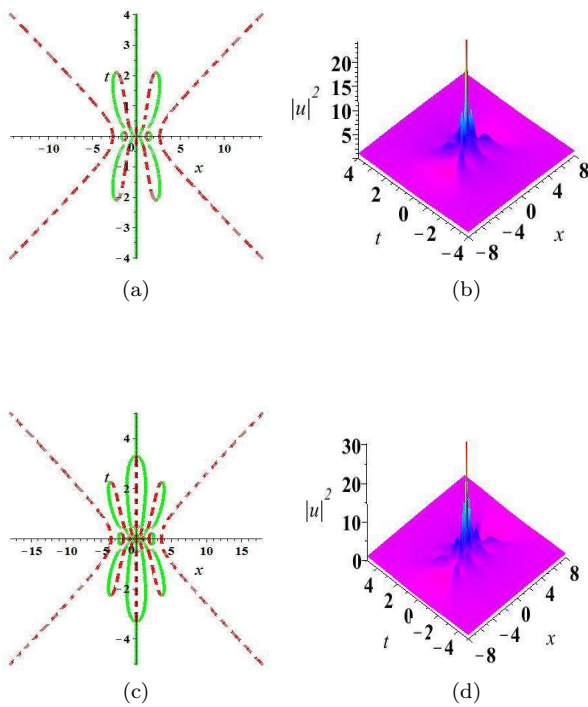


FIG. 6: (color online) (a) The trajectory of the third-order RW which is symmetrical about the x and t axis. (b) The density evolution of the third-order RW. (c) The trajectory of the fourth-order RW which is symmetrical about the x and t axis. (d) The density evolution of the fourth-order RW.

VI. DISCUSSION AND CONCLUSION

We propose a simple representation for generalized RW solution, which can be used to get arbitrary order RW solution and observe its dynamics conveniently. Based on the solution, we investigate the trajectories of them though defining the properties function. We find that the fundamental RW has an “X” shaped trajectory. Although the perturbation for RW is weak long before the moment when highest peak emerge, short-time prediction could be realized through measuring the width between the small valleys. The time can be extended with the improvement of measurement precision. For higher-order RW, the whole trajectory is similar to the fundamental one’s. But they are different near the moment when the highest peak emerges, such as the trajectories of the third-order and fourth-order RW in Fig. 6. We just show that there are some differences between them here. The explicit differences need further analysis and could be used to estimate the broken force of the RW in related systems.

Acknowledgments

This work is supported by the National Fundamental Research Program of China (Contact 2011CB921503), the National Science Foundation of China (Contact Nos. 11274051, 91021021).

[1] V. Ruban, Y. Kodama, M. Ruderman, et al., *Eur. Phys. Journ. Special Topics* **185**, 5-15 (2010).
 [2] N. Akhmediev and E. Pelinovsky, *Eur. Phys. J. Special Topics* **185**, 1 (2010).
 [3] C. Kharif and E. Pelinovsky, *Eur. J. Mech. B/Fluids* **22**, 603 (2003).

[4] A. R. Osborne, *Nonlinear Ocean Waves* (Academic Press, New York, 2009).
 [5] E. Pelinovsky and C. Kharif, *Extreme Ocean Waves* (Springer, Berlin, 2008).
 [6] D.R. Solli, C. Ropers, P. Koonath, B. Jalali, *Nature* **450**, 06402 (2007).

- [7] A. Chabchoub, N.P. Hoffmann, and N. Akhmediev, Phys. Rev. Lett. **106**, 204502 (2011).
- [8] A. R. Osborne, Mar. Struct. **14**, 275 (2001); N. Akhmediev, A. Ankiewicz, M. Taki, Phys. Lett. A **373**, 675-678 (2009).
- [9] B. Kibler, J. Fatome, C. Finot, G. Millot, et al., Nature Phys. **6**, 790 (2010).
- [10] N. Akhmediev, A. Ankiewicz, J.M. Soto-Crespo, Phys. Rev. E **80** 026601 (2009).
- [11] Y. Ohta, J.K. Yang, Proc. R. Soc. A **468**, 1716-1740 (2012).
- [12] B.L. Guo, L.M. Ling, Q. P. Liu, Phys. Rev. E **85**, 026607 (2012).
- [13] B. Guo, L. Ling, Chin. Phys. Lett. **28**, 110202 (2011).
- [14] B. Guo, L. Ling and Q. P. Liu, Stud. Appl. Math. **130**, 317-344 (2013).
- [15] V. Matveev and M. Salle, *Darboux transformation and solitons*, Springer-Verlag, Berlin (1991).
- [16] C.-L. Terng and K. Uhlenbeck, Comm. Pure Appl. Math. **53**, 1-75 (2000).
- [17] V.E. Zakharov, and S.V. Manakov, Sov. Phys. JEPT Lett. **18**, 243 (1973).
- [18] P. Dubard, P. Gaillard, C. Klein, V.B. Matveev, The European Physical Journal Special Topics **185**, 247-258 (2010)
- [19] P. Gaillard, J. Phys. A: Math. Theor. **44**, 435204 (2011)
- [20] C Kalla, J. Phys. A: Math. Theor. **44**, 335210 (2011)
- [21] D. H. Peregrine, J. Aust. Math. Soc. Ser. B **25**, 16-43 (1983).
- [22] L.C. Zhao, Ann. Phys. **329**, 73-79 (2013).
- [23] N. Akhmediev, A. Ankiewicz, J.M. Soto-Crespo, and J.M. Dudley, Phys. Lett. A **375**, 541-544 (2011).